Stereocomplex Formation in Polylactide Multiarm Stars and Comb Copolymers with Linear and Hyperbranched Multifunctional PEG

Jeannette Geschwind, Sahas Rathi, Christine Tonhauser, Martina Schömer, Shaw Ling Hsu, E. Bryan Coughlin,* Holger Frey*

A systematic comparison between graft poly(L-lactide) copolymers with different topologies and their ability to form stereocomplexes with poly(D-lactide) (PDLA) is performed. Comb and hyperbranched copolymers based on functional poly(ethylene glycol) and poly(L-lactide) with molecular weights in the range of 2000–90 000 g mol^{-1} and moderate molecular weight distributions ($\overline{M}_w/\overline{M}_n$ = 1.08–1.37) are prepared via the combination of anionic and ring-opening polymerization. Two "topological isomers," a linear poly(ethylene oxide)/poly(glycerol) (PEG/PG) copolymer and a branched PEG/PG copolymer are used as backbone polymers. Furthermore, the stereocomplex formation between PDLA and the hyperbranched and comb copolymers containing poly(L-lactide) arms is studied. Stereocomplex formation is confirmed by DSC as well as by Fourier transform IR (FTIR) and Raman spectroscopy.

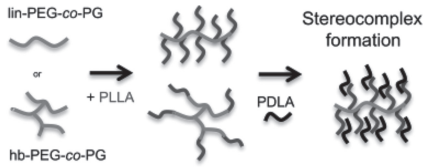

1. Introduction

Copolymers of poly(lactide) (PLA) and poly(ethylene glycol) (PEG) have attracted increasing attention since they offer a unique combination of biodegradability, biocompatibility, and hydrophilicity. They have been extensively studied since publication of seminal reports by several groups including Younes and Cohn in 1987.[1–4] A common method for the preparation of these systems is by using coordination–insertion ring-opening polymerization of lactide using $Sn(Oct)_2$ as the catalyst and PEG containing hydroxyl end groups as a macroinitiator to obtain linear block copolymers. Furthermore star-shaped,[5–7] tree-shaped,[8] and graft copolymers have been described.[9–12]

Branched polylactides have been synthesized, for example, by using pentaerythritol as an initiator yielding star-shaped PLA.[13] Hedrick and co-workers[14]prepared well-defined star PLAs with up to 12 arms using multifunctional dendritic initiators derived from 2,2′-bis(hydroxymethyl)-propionic acid derivatives and Finne and Albertson[15] used a spirocyclic tin catalyst to realize star-shaped poly(L-lactide) (PLLA). Star-shaped PLA polymers with different comonomers, for example glycolide, are well described in the literature.[16–18] For example Vidovic et al.[19] and Kissel et al.[20] used poly(vinyl alcohol), which is hydrophilic, soluble in water, and nontoxic to prepare graft-copolymers with PLA side chains that have also been tested as drug delivery systems. Xi and co-workers[21] synthesized star-shaped PLA starting from hydroxyl-terminated poly(amido amine) (PAMAM) dendrimer cores. Frey and co-workers[22] employed well-defined hyperbranched polyglycerols with narrow polydispersity and adjustable molecular weight.

J. Geschwind,[+] Dr. C. Tonhauser, Dr. M. Schömer, Prof. H. Frey
Institute of Organic Chemistry, Organic and Macromolecular Chemistry, Duesbergweg 10–14, Johannes Gutenberg-Universität Mainz, D-55099 Mainz, Germany
E-mail: hfrey@uni-mainz.de
S. Rathi, Prof. S. L. Hsu, E. B. Coughlin
Polymer Science and Engineering Department, University of Massachusetts Amherst, Amherst, MA 01003
E-mail: Coughlin@mail.pse.umass.edu
[+]Present address: Graduate School Material Science in Mainz, Staudinger Weg 9, D-55128 Mainz, Germany

DOI: 10.1002/macp.201300074

Blends of PLLA and poly(D-lactide) (PDLA) form stereocomplex crystallites with a distinct crystal structure, which melts at approximately 230 °C. The high melting temperature is attributed to strong van der Waals interactions that cause a specific energetic interaction-driven packing.[23,24] Hence, this stereocomplex has received attention for potential high performance biodegradable materials. Different methods for stereocomplex formation are described in literature.[25–37] The relevant parameters for stereocomplexation of PLLA and PDLA have been reported as well, including molecular weight of the constituents, mixing ratio, optical purities, and crystallization time and temperature.[23,38–40] For example, thermal properties and crystallization behaviors of PLA and its enantiomeric blends have been analyzed by Opaprakasit et al.[41] The crystalline morphologies of PDLA/PLLA blends with equal molecular weight have been extensively studied.[39,42] Furthermore, Hillmyer and coworkers[43] studied poly(D-lactide)-poly(menthide)-poly(D-lactide) triblock copolymers as crystal nucleating agents for poly(L-lactide), and Li and Vert[44] studied stereocomplex-induced gelation of PEG-PLLA block copolymers.

There have been no studies in the literature dedicated to the influence of architecture on stereocomplex crystallization. The availability of the varied architecture PLLA-based copolymers provides an opportunity to study the impact of polymer architecture on PLA stereocomplex formation. In this work, PEG-PLLA copolymers using PEG core molecules with different topologies were synthesized and characterized using NMR spectroscopy, FTIR spectroscopy, GPC, and DSC. Blends of these varied architecture PLLA copolymers with PDLA were prepared and stereocomplex formation was studied to understand the impact of polymer architecture on PLA stereocomplex formation. The crystallization behavior of these blends was studied using isothermal and non-isothermal crystallization experiments.

2. Experimental Section

2.1. Instrumentation

2.1.1. NMR Spectroscopy

^{1}H NMR spectra (300 MHz and 400 MHz) and ^{13}C NMR spectra (75.5 MHz) were recorded using a Bruker AC300 or a Bruker AMX400 spectrometer. All of the spectra were referenced internally to residual proton signals of the deuterated solvent at room temperature.

2.1.2. Size Exclusion Chromatography

Size-exclusion chromatography (SEC) of the samples was performed in DMF containing 0.25 g L^{-1} of lithium bromide. An Agilent 1100 Series GPC Setup was used, including a PSS HEMA column ($10^6/10^5/10^4$ g mol^{-1}), and both UV (254 nm) and RI detectors. Calibration was performed with poly(ethylene oxide) (PEO) standards provided by Polymer Standards Service (PSS). The eluent was generally used at 50 °C at a flow rate of 1 mL min^{-1}.

2.1.3. Differential Scanning Calorimetry

Differential scanning calorimetry (DSC) measurements were carried out using a Perkin–Elmer Thermal Analysis Controller TAC 7/DX in a temperature range from –100 to 200 °C, using heating rates of 4 and 10 K min^{-1}.

2.1.4. FTIR Spectroscopy

FTIR spectra were recorded on a Thermo Scientific iS10 FTIR spectrometer, equipped with a diamond ATR unit and on a Perkin–Elmer Spectrum 100 FTIR spectrometer equipped with a universal ATR unit.

2.1.5. Raman Spectroscopy

A Jobin–Yvon Horiba LabRam HR800 dispersive Raman spectrometer was used to obtain Raman spectra of the samples. The 632.8 nm line of a helium–neon gas laser was used for excitation. Spectral resolution of less than 4 cm^{-1} was maintained near the laser line.

2.1.6. Optical Microscopy

Spherulite growth in the PDLA/PLLA-copolymer blends was observed using an Olympus (Tokyo, Japan) polarized optical microscope (BH-2) equipped with a heating stage. The samples for optical observation were prepared by the following procedure. First, a sample of approximately 8 mg was placed between a glass slide and a Kapton film. The sample was heated to melt completely, it was then pressed to obtain a thin film and then cooled to room temperature. Subsequently, the sample was again melted and transferred to the hot stage maintained at 160 °C. All crystallization experiments were monitored using the birefringence developed for samples between two polarizers with an orthogonal polarization axis. Images of the spherulites and morphologies were taken with a digital camera.

2.2. Materials

All of the reagents and solvents were purchased from Acros and used as received, if not mentioned otherwise. Deuterated DMSO-d_6 and $CDCl_3$ were purchased from Deutero GmbH. Ethoxyethyl glycidyl ether (EEGE) was prepared as described by Fitton et al.,[45] dried over CaH_2, and freshly distilled before use. *N,N*-Dibenzyl-2-aminoethanol was synthesized as reported previously.[46] L-Lactide (LLA) (98%; Aldrich Chemical Co.) and stannous(II)-2-ethylhexanoate ($Sn(Oct)_2$) (95%, Aldrich Chemical Co.) were used as received.

2.3. Synthesis

Random copolymers of EO and glycidol as well as random copolymers of EO and EEGE were prepared as described previously.[47,48]

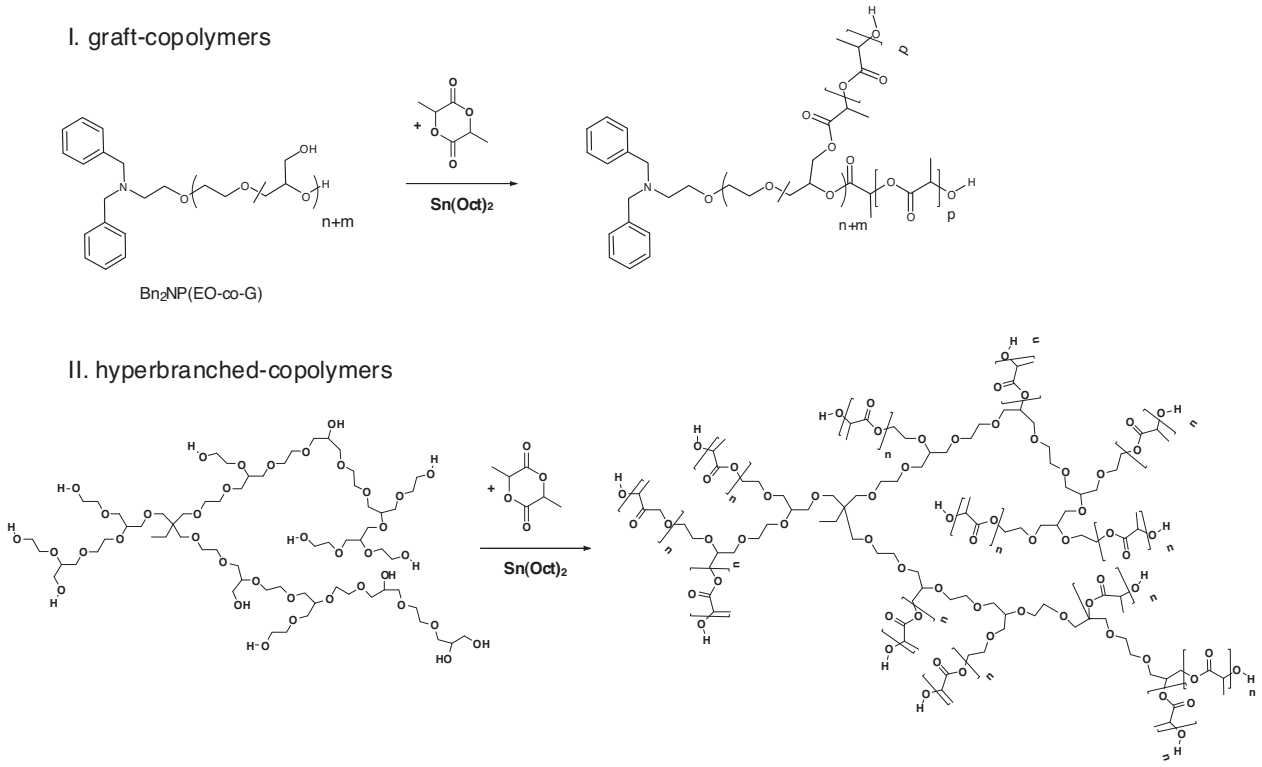

Scheme 1. Synthesis of graft-PEG/PLLA copolymers based on functional PEG copolymers of different topology; top: linear; bottom: hyperbranched.[47–49]

2.3.1. Lactide Polymerization

The general synthetic procedure is exemplified for the graft copolymers (sample 13) and was performed in an analogous manner for all other linear, star, and hyperbranched copolymers prepared. The multifunctional backbone polymer PEG ($\overline{M}_n$ = 12 000 g mol^{-1}) 0.5 g was dried under vacuum for at least 4 h in a Schlenk tube (reaction vessel). L-lactide (2.88 g, 20 mmol) was added, melted at 120 °C, and stirred under nitrogen atmosphere. Subsequently, the required amount of $Sn(Oct)_2$ catalyst (0.007 mL, 0.02 mmol, as a 10 vol% solution in toluene) was injected into the reaction vessel. Stirring was continued, and after 8 h, the reaction mixture was solidified. At the end of the reaction, the mixture was allowed to cool. The solid product was dissolved in chloroform (20 mL), precipitated in hexane, and dried in vacuo. In some cases, analysis of the copolymers by SEC showed a minor low molar mass fraction or some unreacted monomer that could be removed by dialysis in chloroform (benzoylated dialyzing tubes (Sigma Aldrich), MWCO 1000 g mol^{-1}). The yields generally exceeded 90%.

2.3.2. Blend Preparation

Blends of the PLLA copolymers and PDLA were prepared by separately dissolving each component in dichloromethane. The two solutions were then mixed in the desired compositions and stirred vigorously. After 2 h, the mixture was precipitated into a tenfold excess of cold hexane. The solid blend was filtered and dried in vacuo for at least 12 h.

3. Results and Discussion

3.1. Synthesis of the Copolymers

In this investigation, multifunctional PEO copolymers with varying glycerol content and different topology were used to synthesize graft- or star-copolymers. Depending on the amount of hydroxyl functionalities, the number of side chains can be varied. Different PLA chain lengths were obtained by varying the monomer to hydroxyl group ratio. The synthesis of the copolymers was achieved via a core-first approach, performing controlled ring-opening polymerization of L-lactide on a multifunctional polyether used as an initiator backbone polymer. For linear graft-copolymers, the macroinitiator is synthesized from EO and EEGE. Acidic removal of the ethoxyethyl protecting group yielded linear P(EO-*co*-G), which, compositionally, is a linear PEG with a varying number of hydroxyl groups, where lactide polymerization can be initiated. On the other hand, the hyperbranched macroinitiator is prepared via direct copolymerization of glycidol and ethylene oxide (Scheme 1).

Characterization of PLLA stars based on hyperbranched PEO was already described in a recent work.[47] *Hb67* P(EO-*co*-G), for example, stands for a hyperbranched PEO with 67 hydroxyl groups (samples 17–19), *hb128* P(EO-*co*-G)

Table 1. Comparison of molecular weights obtained from NMR spectroscopy and SEC of the graft-copolymer samples.

No.	Sample	LLA units[a)]	$\overline{M}_n$ (SEC)[b)] [g mol^{-1}]	PDI (SEC)
1	$Bn_2NP(EO_{335}$-*co*-$G_{11})$		6200	1.17
2	$P((EO_{335}$-*co*-$G_{11})$-*g*-LLA_{97}	97	69 000	1.13
3	$Bn_2NP(EO_{234}$-*co*-$G_{26})$		5400	1.16
4	$P((EO_{234}$-*co*-$G_{26})$-*g*-$LLA_{38})$	38	41 000	1.28
5	$P((EO_{234}$-*co*-$G_{26})$-*g*-$LLA_{22})$	22	24 000	1.37
6	$Bn_2NP(EO_{71}$-co-$G_{28})$		2000	1.20
7	$P((EO_{71}$-co-$G_{28})$-*g*-LLA_{18}	18	10 000	1.28
8	$Bn_2NP(EO_{193}$-*co*-$G_{32})$		4400	1.29
9	$P((EO_{193}$-*co*-$G_{32})$-*g*-$LLA_{48})$	48	54 000	1.14
10	$P((EO_{193}$-*co*-$G_{32})$-*g*-$LLA_{22})$	22	37 000	1.33
11	$Bn_2NP(EO_{307}$-*co*-$G_{90})$		6700	1.19
12	$P((EO_{307}$-*co*-$G_{90})$-*g*-$LLA_{68})$	68	82 000	1.17
13	$P((EO_{307}$-*co*-$G_{90})$-*g*-$LLA_{28})$	28	51 000	1.08
14	*hb128* P(EO-*co*-G)		25 000	1.79
15	*hb128*-P((EO-*co*-G)-*g*-LLA_{42})	42	90 000	1.13
16	*hb128*-P((EO-*co*-G)-*g*-LLA_{24})	24	67 000	1.21
17	*hb67* P(EO-*co*-G)		16 000	1.96
18	*hb67*-P((EO-*co*-G)-*g*-LLA_{42})	42	85 000	1.12
19	*hb67*-P((EO-*co*-G)-*g*-LLA_{20})	20	59 000	1.17

[a)]Determined by ^{1}H NMR and ^{13}C NMR spectroscopy (hyperbranched samples); [b)]In DMF vs. PEG-standards using the RI detector.

for a hyperbranched PEO with 128 hydroxyl groups (samples 14–16), respectively. For the hyperbranched samples, polymerizations of L-lactide with $Sn(Oct)_2$ did not reach full conversion (about 90%) due to solidification of the reaction mixture. Residual monomer was therefore removed by dialysis in chloroform.

The polymers were characterized by NMR spectroscopy and SEC, as summarized in Table 1.

In Figure 1, the ^{1}H NMR spectrum of sample 10 ($P((EO_{234}$-*co*-$G_{26})$-*g*-$LLA_{22})$) is shown as an example ($CDCl_3$). In addition to the PEG backbone signal ($\delta = 3.60$ ppm), the resonances for poly(L-lactide) or poly(D,L-lactide) can be found ($\delta = 5.17$ and 1.57 ppm). The lactide side chain length and also the molecular weight were determined by comparison of the integration values from the lactide chain end-group resonances ($\delta = 4.33$ ppm) to those from PLA methine resonances ($\delta = 5.17$ ppm). Other information obtained from the spectrum is whether the reaction proceeds to complete conversion since the resonances of the methine protons in the monomer and the polymer are different. Therefore, monomer signals disappear with complete conversion.

In this case, the side chain lengths for the star-shaped samples with a hyperbranched PEG core could not be calculated from the ^{1}H NMR spectroscopy because the chemical shifts of the PLA end-group signal ($\delta = 4.33$ ppm) and the signal of the hyperbranched core overlap. Instead, inverse gated ^{13}C NMR spectroscopy was used to confirm the structure of the star-shaped copolymer (Figure 2). However, ^{13}C NMR spectroscopy provided further important information for the characterization of the hyperbranched polymers, viz. the lactide side chain degree of polymerization.

For the linear copolymer, no signals assignable to $-O-CH_2CH_2OH$ or $-O-CH_2CH_2OH$ carbon atoms belonging to hydroxyl-terminated PEG groups ($\delta = 18.2$ ppm) were detected. This shows that PEG hydroxyl groups were transformed quantitatively, and no residual PEG copolymer is present in the final product.

The molecular weights ($\overline{M}_n$) for all synthesized copolymers were higher than that of the starting backbone copolymer and the distributions were monomodal (Figure 3). This confirms that the products were not mixtures of different homopolymers, but actually copolymers. The obtained polydispersities were low to moderate (between 1.08 and 1.37), as expected for this type of ring-opening polymerization. In general, a deviation of the molecular weights determined by SEC and the calculated values based on the NMR spectroscopy results was found. The observed effect is due to several reasons. First of all, samples with lactide side chains differ from linear PEO, which was used as a standard polymer for calibration. Furthermore, highly

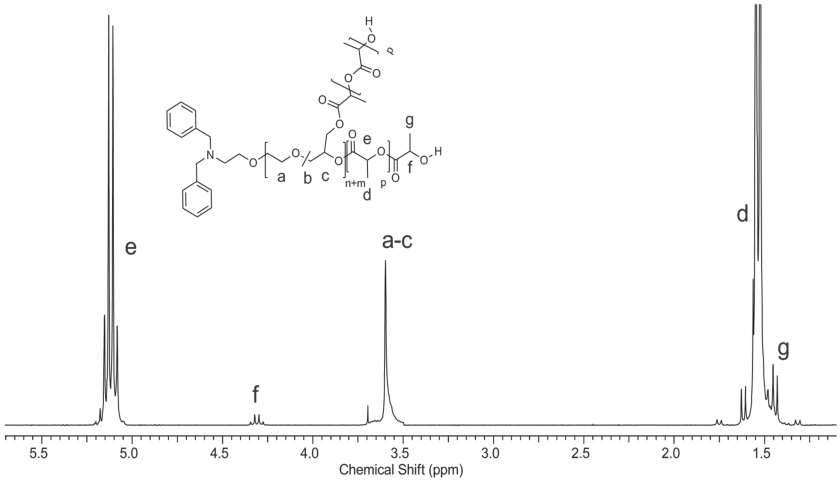

Figure 1. ^{1}H NMR spectroscopy of sample $P((EO_{234}$-*co*-$G_{26})$-*g*-$LA_{22})$ in $CDCl_3$.

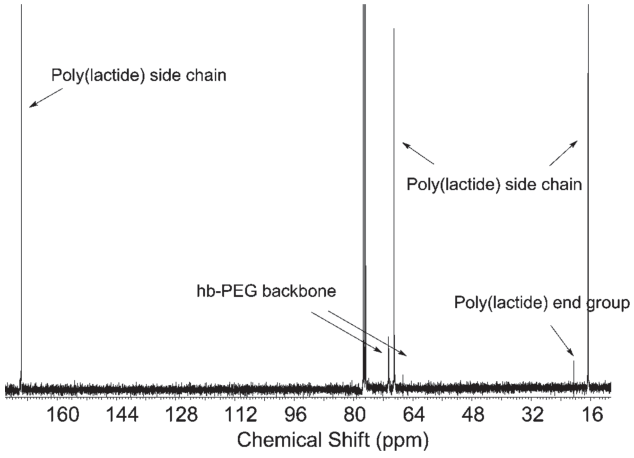

Figure 2. ^{13}C NMR spectrum of sample *hb67*-P((EO-*co*-G)-*g*-LLA_{42}) (sample 18) in $CDCl_3$.

branched or graft architectures were synthesized. The hydrodynamic radius, which determines the elution volume of the polymer, does not increase linearly with the increase in mass. Generally, star-shaped or hyperbranched copolymers show a lower hydrodynamic volume in solution than linear analogues of similar molar mass. This explains why the strongest underestimation of molecular weight is found for the most highly branched systems with the longest side chains. As can be seen for the hyperbranched samples, the PDI decreases after the lactide grafting.

3.2. Thermal Characterization with DSC

The thermal behavior of the prepared copolymers has been quantified by DSC. The results of the second heating scan, glass transition temperature (T_g), melting point, and degree of crystallization of all L-lactide graft-copolymers are shown in Table 2.

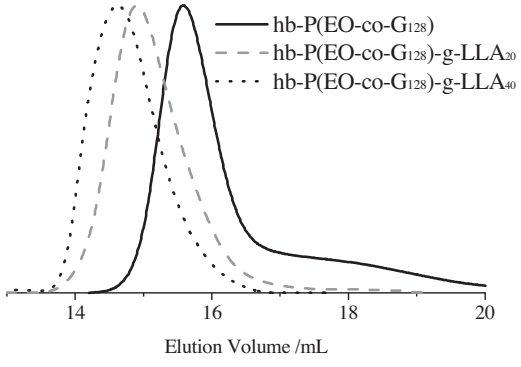

Figure 3. Typical SEC traces of some of the hyperbranched copolymers (samples 14–16) before and after lactide grafting.

Table 2. DSC results of the graft copolymer samples.

No.	Sample	T_g [°C]	T_m [°C]	ΔH_m [J g^{-1}]	χ^c
1	$Bn_2NP(EO_{335}$-*co*-$G_{11})$	–48			
2	P((EO_{335}-*co*-G_{11})-*g*-LLA_{97}	38	159	51.49	0.51
3	$Bn_2NP(EO_{234}$-*co*-$G_{26})$	–59			
4	P((EO_{234}-*co*-G_{26})-*g*-LLA_{38})	36	137	50.30	0.50
5	P((EO_{234}-*co*-G_{26})-*g*-LLA_{22})	29	125	40.27	0.37
6	$Bn_2NP(EO_{71}$-co-$G_{28})$	–56			
7	P((EO_{71}-co-G28)-*g*-LLA_{18}	33	134	28.54	0.31
8	$Bn_2NP(EO_{193}$-*co*-$G_{32})$	–53			
9	P((EO_{193}-*co*-G_{32})-*g*-LLA_{48})	45	158	52.52	0.54
10	P((EO_{193}-*co*-G_{32})-*g*-LLA_{22})	33	146	26.95	0.26
11	$Bn_2NP(EO_{307}$-*co*-$G_{90})$	–49			
12	P((EO_{307}-*co*-G_{90})-*g*-LLA_{68})	42	154	49.23	0.51
13	P((EO_{307}-*co*-G_{90})-*g*-LLA_{28})	39	137	12.97	0.13

In all cases, no T_g or melting point for the PEG or PLLA homopolymer constituents was detected. These results indicate that PEG/PLLA copolymers with no homopolymer contaminants were obtained, as determined by the SEC data.

In general, T_gs and melting points of both star and brush structures increase with increasing amount of polylactide side chains and the side chain degree of polymerization. The melting temperature shifts to a higher temperature with an increasing L-LA/PEG ratio. Compared with pure PLLA (T_m = 170–180 °C), the melting temperatures are lowered for the copolymers. This can be explained by two factors, i) by the backbone polymer affecting the crystallization, and ii) by the molecular architecture of the copolymers. In all samples, the PLA side chain degree of polymerization varies between 14 and 50 lactic acid units. Therefore, oligomers linked to a PEG backbone are present in the samples, and oligomer melting points are, in general, lower than polymer melting points.[50] Similar results were found for the star-shaped samples containing a hyperbranched core, as reported recently.[49]

Star copolymers based on PLLA and PEG showed a decrease in degree of crystallization by increasing the number of branches. As for the graft-copolymers, melting points and T_gs decrease for shorter side chain degree of polymerization. A difference can also be found between the different kinds of branched architectures. The graft-copolymers 2, 4, 5, and 7 showed a higher degree of crystallization than star-shaped copolymers with a hyperbranched core. So, not only the composition but also the architecture of the copolymers affects their thermal

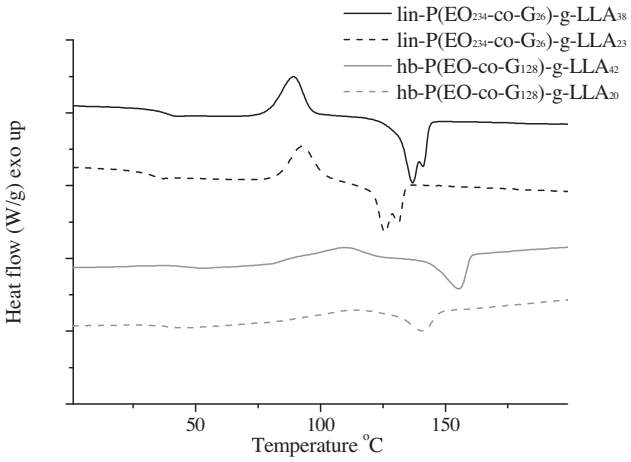

Figure 4. DSC results for some typical graft- and hyperbranched samples.

behavior. The degree of crystallization was calculated from the following equation:

$$\chi^c = \Delta H_m / (\Delta H_m^{\infty} f_w^{LLA}) \quad (1)$$

With ΔH_m as the area under the melting endotherm, f_w^{LLA} as the weight fraction of the PLLA, and ΔH_m^{∞} as the theoretical heat of fusion of the PLLA homopolymer at 100% crystallinity. The ΔH_m value (93 J g^{-1}) was obtained from the literature.[50]

The reduced degree of crystallization with branching is due to an increase in free chain ends, disrupting the fold pattern of the crystal. ΔH_m decreases as the number of arms increases, but increases with longer side chains. This can also be observed by looking at the crystallization peak. Figure 4 shows the DSC curves for two graft-copolymers and two hyperbranched samples containing poly(L-lactide) side chains. For the graft-copolymers, the crystallization peak is very sharp and occurs at lower temperatures, whereas for the hyperbranched samples, the crystallization peak is broad. This can be explained by the hyperbranched topology. In the hyperbranched samples, not all side chains are located at the exterior of the polymer because hyperbranched PEG contains some hydroxyl groups in the interior. Consequently, the growing polylactide side chain cannot easily adopt conformations that permit interaction with other chains. The interaction between the PLA side chains is reduced because of a more open star structure for highly branched architectures. It was noted that the melting peak was broadened, as the degree of branching increased. This was more pronounced for the hyperbranched copolymers compared with the graft-copolymers (Figure 4). Two melting endotherms are observed in most of the graft-copolymers. This phenomenon has been interpreted by the presence of two different crystal structures, α and the less stable α′ structure.[50]

The crystallization and T_g of the PEG within the copolymers are not detected in the DSC traces because of its low mass fraction. Both PEG and PLLA are able to crystallize and the crystallization behavior of crystalline–crystalline block copolymers is sophisticated. Several studies report that PEG and poly(L-lactide) are partially miscible, so no phase separation occurs.[51,52] Because of this only one melting point and one glass transition, lying between that of the two homopolymers, can be detected, as can be seen in Table 3.

3.3. Blending and Stereocomplexation

To study the influence of the prepared copolymers for lactide homopolymer materials, a blend was prepared. For blend preparation, solution mixing was used. Three different copolymers with a constant degree of polymerization for the polylactide side chains of about 40 lactic acid units and similar molecular weights of the PEG macroinitiator ($\overline{M}_n \approx 12\,000$ g mol^{-1}) and PDLA homopolymer (30 000 g mol^{-1}) were used for blending.

The following abbreviations were used to simplify the blend names. P($(EO_{234}$-*co*-$G_{26})$-*g*-LLA_{38}) is $graft_{10}$, P($(EO_{193}$-*co*-$G_{32})$-*g*-LLA_{48}) is $graft_{15}$ and hb_{67}-P((EO-*co*-G)-*g*-LLA_{40}) is hb_{20}. The subscript numbers indicate the amount of glycerol monomers in wt% (glycerol either linear or branched) present in the backbone of the copolymer. Furthermore, a triblock copolymer with PEG mid-block and polylactide end-blocks was used for blending to compare the different architectures. The compositions of the blends prepared are shown in Table 3. As it can be seen from Table 3,

Table 3. Composition of the blends prepared.

No.	Name	Architecture	Glycidol units	Blend PEG content [wt%]	Blend PLLA content [wt%]
A	PDLA/tribl(25%)	Triblock	0	17.50	7.50
B	PDLA/$graft_{10}$(25%)	Graft	10	1.75	23.25
C	PDLA/$graft_{15}$(25%)	Graft	15	1.25	23.75
D	PDLA/hb_{20}(25%)	Hyperbranched	20	2.00	23.00
E	PDLA/tribl(40%)	Triblock	0	28.00	12.00
F	PDLA/$graft_{10}$(40%)	Graft	10	2.80	37.20
G	PDLA/$graft_{15}$(40%)	Graft	15	2.00	38.00
H	PDLA/hb_{20}(40%)	Hyperbranched	20	3.20	36.80

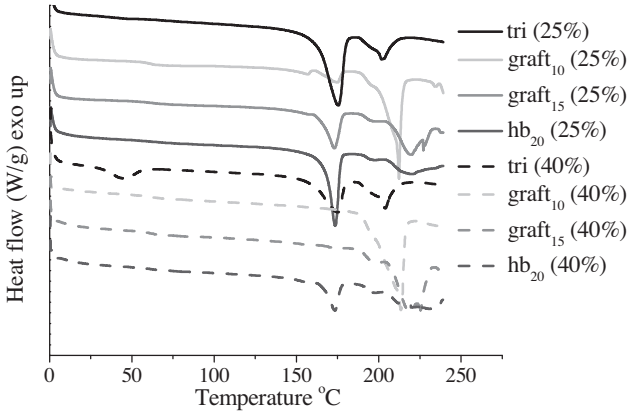

Figure 5. DSC traces of as precipitated blends (first heating).

the graft$_{10}$, graft$_{15}$, and hyperbranched blends containing similar amounts of PEG and PLLA and allowed for the investigation of the impact of polymer architecture on stereocomplex formation. The triblock blends contain much higher amounts of PEG and lower amounts of PLLA. Thus, the PLLA/PDLA ratio is similar in the first three blends, while it is much lower in the triblock copolymer/PDLA blends.

3.4. Analysis of the As-precipitated Blends

In order to analyze the structure of the blends formed upon solution precipitation, DSC was performed on the as-precipitated blends (Figure 5). Stereocomplex formation between PDLA and PLLA can be studied by DSC since the stereocomplex melting point is about 50 °C higher than that of pure PLA homopolymer. Quantitative information on the thermal behavior can be obtained by comparing the melting enthalpies of the stereocomplex crystals and the homopolymer crystals. As it can be seen from the melting enthalpy of the homopolymer crystals and stereocomplex crystals in Figure 5, a mixture of stereocomplex crystals and homopolymer crystals is formed in the case of 25% blends. Because of the low content of PLLA in the triblock copolymer blend, the amount of stereocomplex crystals is lower than the amount of triblock crystals. For the graft$_{10}$, graft$_{15}$, and hyperbranched blends, the amount of stereocomplex crystals decreases and homopolymer crystals increases with increase in graft density indicating that stereocomplex formation is hindered with increasing graft density. In the case of 40% blends, only the stereocomplex crystals are formed in the graft$_{10}$ and graft$_{15}$ blends while both stereocomplex and homopolymer crystals are formed in the case of hyperbranched blends. From the DSC data on the as-precipitated blends, we can conclude that stereocomplex formation during solution precipitation is hindered with increasing graft density and branching.

3.5. Blend Crystallization

3.5.1. Non-isothermal Crystallization

In order to further study the influence of polymer architecture on stereocomplex formation, isothermal, and non-isothermal crystallization experiments was performed. The non-isothermal crystallization experiment was performed in the DSC. The as-precipitated blends were heated above the melting point of the stereocomplex to erase the thermal history, cooled at 20 K min^{-1} to 0 C and then reheated to evaluate the extent of the crystal formation during the cooling cycle. The results of the second heating scan are shown in Table 4 and Figure 6.

All the prepared blends, regardless of the topology of the functional PEG, showed stereocomplex formation and an elevated melting point between 194 and 220 °C. Depending on PLLA/PDLA ratio, different amounts of stereocomplex crystals are formed. In theory, for equimolar blends with $\chi_D = 0.5$, the melting enthalpy of stereocomplex crystallites reaches its maximum and decreases with a deviation of χ_D from 0.5 and the melting enthalpy of homocrystallites increases. The mixing ratio χ_D is defined as follows:

$$\chi_D = \text{Weight of PLLA}/(\text{Weights of PLLA plus PDLA}) \quad (2)$$

The data suggest that the melting enthalpy for stereocomplex crystallites is always higher for the 40% blends than for the 25% since more PLLA is present in the latter samples, so the mixing ratio is closer to 0.5. In the graft-copolymer blends with 40% copolymer as well as in the hyperbranched copolymer blends with 40% copolymer,

Table 4. DSC results for all prepared blends. (second heating run; heating rate of 20 °C min^{-1} was used. The measured temperature range was from 0 to 250 °C (for some samples only 240 °C, due to degradation of the sample at higher temperatures)).

No.	Sample	T_g [°C]	T_{m1} [°C]	T_{m2} [°C]	ΔH_{m1} [J g^{-1}]	ΔH_{m2} [J g^{-1}]
A	PDLA/tribl(25%)	X	169	200	23	9
B	PDLA/tribl(40%)	X	168	200	24	9
C	PDLA/graft$_{10}$(25%)	49	162	201	3	29
D	PDLA/graft$_{10}$(40%)	45	X	194	X	41
E	PDLA/graft$_{15}$(25%)	46	165	221	13	26
F	PDLA/graft$_{15}$(40%)	44	X	220	X	54
G	PDLA/hb$_{20}$(25%)	54	X	212	X	4
H	PDLA/hb$_{20}$(40%)	51	X	209	X	22

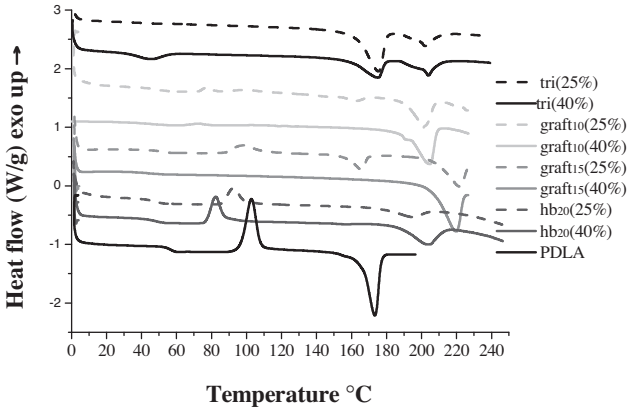

Figure 6. DSC results for all prepared blends (second heating scan).

the mixing ratio is almost 0.4, as the blends contain less than 2% PEG backbone polymer. Because of the high PLLA/PDLA ratio, only the stereocomplex crystals are formed in the graft-copolymer blend samples. In the case of hyperbranched copolymer blends, despite a similar PLLA/PDLA ratio to the graft copolymer blends, stereocomplex melting enthalpy is much lower than the graft copolymer blends. Moreover, the stereocomplex crystallization occurs during the heating cycle in the hyperbranched copolymer blends, indicating that stereocomplex crystallization is hindered in these blends as the stereocomplex crystallization could not occur during the cooling cycle like in the other blends.

The triblock copolymer blends showed a different behavior as the amount of PEG is very high compared with the graft- and hyperbranched copolymer blends. For the triblock copolymer blends, two melting peaks are observed, as for the graft and hyperbranched blends. However, the melting enthalpy of the homopolymer is considerably higher than the melting enthalpy for stereocomplex melting. This suggests that less stereocomplex is formed. In these blends, the PLLA/PDLA ratio is low, leading to less stereocomplex formation and more homopolymer crystallization. A third melting point at around 50 °C was observed in the 40% triblock copolymer blend. This melting point can be assigned to the PEG melting since the amount of PEG in the blend is about 28%.

The hindrance for stereocomplex crystallization observed experimentally in the case of hyperbranched copolymer blends can be explained by the following hypotheses, which are mainly based on steric effects introduced by the densely branched structure. First, some polylactide chains are located in the center of the hyperbranched core and are not accessible for stereocomplex formation with the surrounding PDLA. Furthermore, there are many side chains connected to a rather small core, so steric hindrance may cause limited accessibility for stereocomplexation formation.

3.5.2. Isothermal Crystallization

The crystalline morphology and the spherulitic growth process of all blends were investigated by polarized optical microscopy (POM). Thin-film samples were prepared by isothermal crystallization at 160 °C. For the homopolymer, large spherulites with an average radius of about 2 mm and typical Maltese Cross pattern were formed. In general, if nucleation is slow and crystal growth is fast, only few large spherulites are formed. For the prepared samples, two different kinds of morphologies were formed, viz. spherulitic and dendritic morphologies, as it can be seen from Figure 7. Figure 7B is what may be called a classic spherulite, with bright contrast deriving from birefringence indicating a crystalline entity. Spherulites have the same crystallographic axis along every radius, whereas dendrites, which are also highly branched, possess a common single crystal orientation (Figure 7A). The crystallization behavior and the morphology of PLLA depend on both the nucleation activation and the mobility of chain segments.

Figure 8 shows the morphologies formed by isothermal crystallization of the prepared blends. As expected, for all

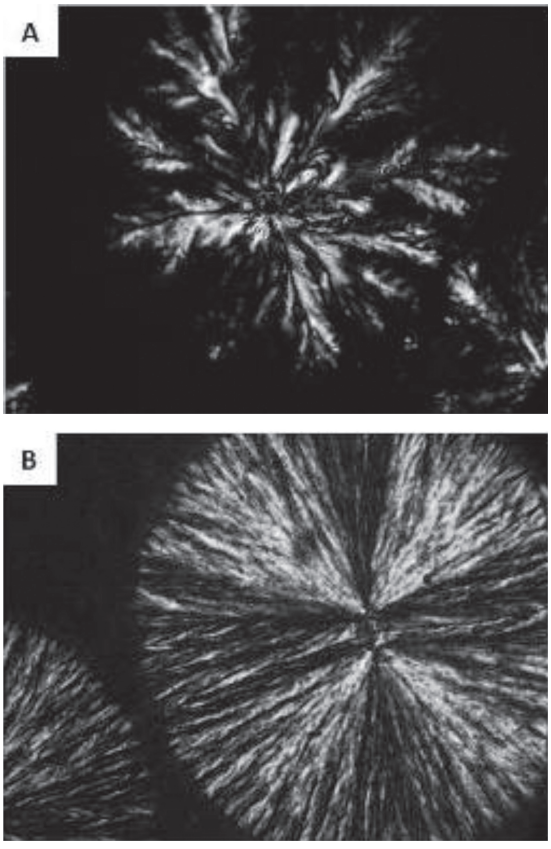

Figure 7. A) Dendritic morphology grown from a triblock copolymer blend (Table 2 entry B). B) Spherulites grown from a 40% blend hyperbranched sample (Table 2 entry H).

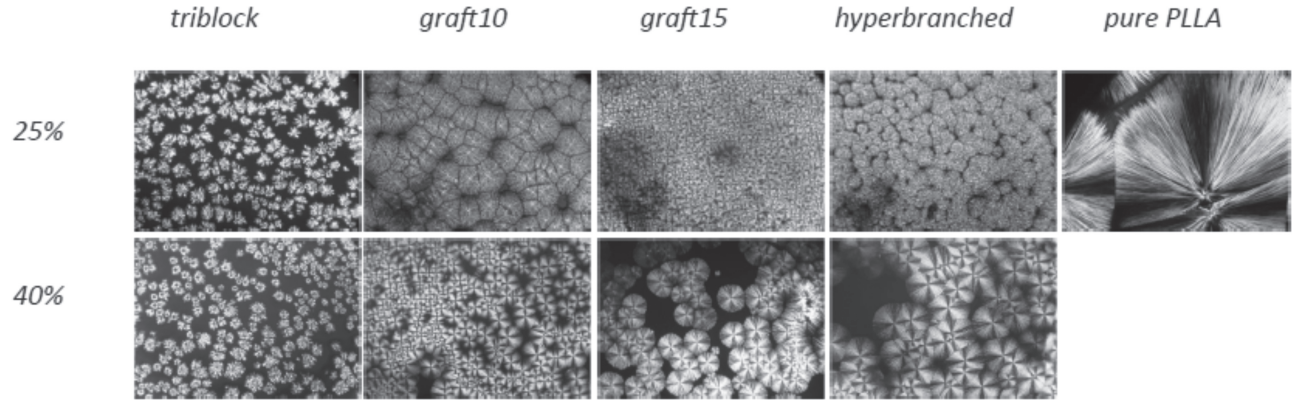

Figure 8. Spherulites of the blends containing 25% and 40% copolymer (Isothermal crystallization at 160 °C) compared with pure PDLA.

samples, smaller spherulites/dendrites compared with the homopolymer were formed.

It can be seen that most of the 40% blend samples and some of the 25% blend samples show a typical spherulitic morphology. For all the triblock copolymer blends and the hyperbranched and graft$_{10}$ 25% blends, no clear Maltese cross patterns were observed. The morphology of the 25% hyperbranched blend samples differs from the other samples.

Raman spectroscopy mapping on the crystallites proves that the crystals are entirely composed of racemic crystallites except in the case of 25% hyperbranched copolymer blend (Figure 9). The isothermal crystallization experiment coupled with Raman spectroscopy mapping proves that in all the blends apart from the 25% hyperbranched copolymer blend, stereocomplex crystallization occurs preferentially to homopolymer crystallization. In the case of 25% hyperbranched copolymer blend because of the increased steric hindrance, stereocomplex formation is impeded and both homopolymer crystallization and stereocomplex crystallization occur (Figure 9).

The triblock copolymer blends do not show spherulitic morphologies. Instead they form typical dendritic morphologies because of the presence of large amounts of PEG in this blend, which because of its covalent bonds with the PLLA is trapped in the interlamellar and interfibrillar regions of stereocomplex crystals. Numerous interspherulitic amorphous regions are also found in the triblock copolymer blend. This translates to stereocomplex crystals dispersed in a continuous amorphous phase. Raman spectroscopy mapping on the continuous amorphous phase indicates that the amorphous region contains amorphous PDLA and the non-crystallized triblock copolymer. The lower content of PLLA in these blends compared with the hyperbranched and graft copolymer blends results in fewer nucleation sites for stereocomplex crystallization, leading to a different morphology in comparison with the other blends. A

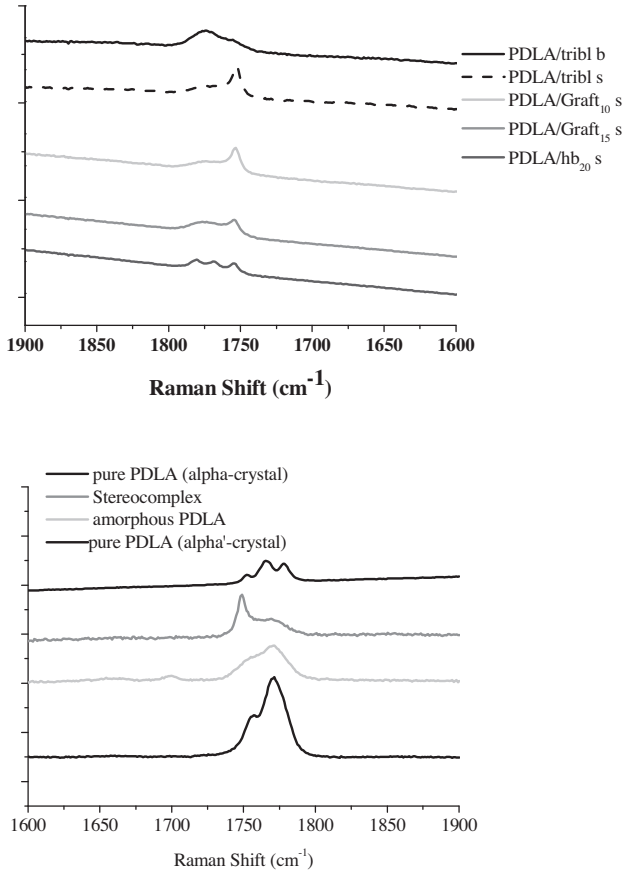

Figure 9. Raman spectroscopy mapping on the 25% blends (top); reference spectra (bottom).

recent paper has reported that such morphological features can enhance the mechanical properties of semicrystalline PLA.[34]

Due to the small amount of PEG core molecules in the graft and hyperbranched samples, PEG could not be detected by Raman spectroscopy. However, since only stereocomplex crystallization takes place and the PEG chains are

connected to the PLLA side chains, the core molecules must be present in the intraspherulitic amorphous regions. Comparing the different blends, more isotropic (black) regions are obtained for samples with higher PEG content. By using POM, it could be confirmed that spherulites formed under non-equimolar conditions are more defective in crystalline structure or more irregular in orientation of the lamellae than those formed under equimolar conditions.

3.5.3. Raman Spectroscopy Mapping

Raman spectroscopy was used to map the composition of the different regions obtained by isothermal crystallization of thin films of the blends at 160 °C. Kister and coworkers observed spectral changes in peak shapes upon PLA stereocomplexation.[53,54] The C=O stretching mode is especially sensitive to the packing and the conformation of the PLA chain.

For pure crystalline PDLA (α-crystal), this peak splits into components corresponding to A, B, E_1, and E_2 modes. A, B, E_1, and E_2 modes are Raman spectroscopy active, whereas only A and E_1 modes are IR active. These modes are observed at 1749, 1763, 1769, and 1773 cm^{-1}. In the case of amorphous PDLA, broad bands are obtained. The spectrum of the pure stereocomplex shows a sharp peak at 1745 cm^{-1} and a broad band at 1760–1780 cm^{-1}. This peak was assigned to the A-type mode corresponding to the fully symmetric vibration.[53]

Raman spectroscopy mapping was performed on the spherulites as well as on isotropic interspherulitic amorphous regions found in the triblock copolymer blends. Figure 9 shows the Raman spectra obtained at the different points for the 25% blends. Spectra obtained from the spherulites are labeled with a suffix "s" and those from the amorphous regions are labeled with a suffix "b". The crystalline regions show the characteristic peaks of the PLA stereocomplex in all blends. The 25% hyperbranched blend crystals, however, exhibit additional bands. Three peaks were obtained, as known from pure crystalline PDLA, but the overall shape was different. The third peak at 1745 cm^{-1} was higher than expected for the α-crystal structure. Thus, this peak seems to be an overlap of the stereocomplex and an α-crystal band. It can be inferred that in the case of 25% hyperbranched blend stereocomplex as well as homopolymer crystallites (α-crystals) are formed. In the case of 40% blends, the crystals in all the blends show peaks characteristic of the stereocomplex crystals. As the PLLA/PDLA ratio is closer to unity in these blends, on isothermal crystallization, stereocomplex crystals were found to be exclusively formed.

4. Conclusion

It was shown that both graft- and star-shaped multi-arm copolymers based on polylactide and PEG/PG copolymers can be synthesized employing the core-first strategy. The average degree of polymerization of PLA arms is adjustable by the monomer/initiator ratio. The occurrence of homopolymerization was observed for some samples, which could be due to traces of moisture in the reaction. For the full structure elucidation of the resulting polymers extensive investigations, including SEC, NMR spectroscopy, DSC and FTIR spectroscopy have been performed.

A systematically varied series of polymers with molecular weights between 10 000 and 90 000 g mol^{-1} was obtained. The molecular weight distribution was narrow for all reactions and the polydispersity index was low for all polymers (between 1.08 and 1.37). It was shown that depending on the side-chain degree of polymerization, the melting point and T_g were decreased compared with pure PLA. The shorter the side chain, the lower the corresponding temperatures. Furthermore, the polymer architecture influences the degree of crystallization of polylactide in the samples, resulting in lower crystallinity for the hyperbranched star-shaped copolymers.

Stereocomplexation of the prepared multiarm graft- and star block copolymers has been studied and compared. Different methods were used to evaluate the PLA stereocomplexation. DSC measurements showed a second and higher melting peak for the stereocomplex at 200–220 °C. Isothermal crystallization experiments were performed to study the blend crystallization. Raman spectroscopy mapping was used to probe the resultant morphology formed. It was found that in all blends except the 25% hyperbranched copolymer blend, stereocomplex crystals formed preferentially over the homopolymer crystals. In the case of triblock copolymer blends, because of the large amount of PEG and small amount of PLLA, a very different morphology was obtained compared with the graft and hyperbranched copolymer blends. Finally, the isothermal and non-isothermal crystallization experiments proved that stereocomplex formation was hindered in the case of hyperbranched copolymer blends. The results of this study are of general importance with respect to polylactide stereocomplexation in complex PLA architectures.

Acknowledgements: J.G. is grateful for a fellowship through the Excellence Initiative (DFG/GSC 266) in the context of the graduate school of excellence "MAINZ" (Materials Science in Mainz) and thanks the Fond der Chemischen Industrie (FCI) for a fellowship.

Received: February 4, 2013; Revised: April 11, 2013; Published online: June 17, 2013; DOI: 10.1002/macp.201300074

Keywords: hyperbranched polymers; poly(lactide); poly(ethylene glycol); ring-opening polymerization; stereocomplexes

[1] H. Younes, D. Cohn, *J. Biomed. Mater. Res.* **1987**, *21*, 1301.
[2] L. T. Lim, R. Auras, M. Rubino, *Prog. Polym. Sci.* **2008**, *33*, 820.
[3] F. P. W. Melchels, J. Feijen, D. W. Grijpma, *Biomaterials* **2009**, *30*, 3801.
[4] C. A. P. Joziasse, H. Veenstra, M. D. C. Topp, D. W. Grijpma, A. J. Pennings, *Polymer* **1998**, *39*, 467.
[5] Y. K. Choi, Y. H. Bae, S. W. Kim, *Macromolecules* **1998**, *31*, 8766.
[6] Y. Lemmouchi, M. C. Perry, A. J. Amass, K. Chakraborty, E. Schacht, *J. Polym. Sci., Part A: Polym. Chem.* **2007**, *45*, 3966.
[7] Y. Li, T. Kissel, *Polymer* **1998**, *39*, 4421.
[8] L. Izzo, D. Pappalardo, *Macromol. Chem. Phys.* **2010**, *211*, 2171.
[9] B. Jeong, K. M. Lee, A. Gutowska, Y. H. An, *Biomacromolecules* **2002**, *3*, 865.
[10] Q. Wang, Y. Wang, *J. Polym. Res.* **2011**, *18*, 385.
[11] Y. Xia, B. D. Olsen, J. A. Kornfield, R. H. Grubbs, *J. Am. Chem. Soc.* **2009**, *131*, 18525.
[12] D. J. Darensbourg, W. Choi, O. Karroonnirun, N. Bhuvanesh, *Macromolecules* **2008**, *41*, 3493.
[13] S. H. Kim, Y.-K. Han, K.-D. Ahn, Y. H. Kim, T. Chang, *Makromol. Chem.* **1993**, *194*, 3229.
[14] B. Atthoff, M. Trollsås, H. Claesson, J. L. Hedrick, *Macromol. Chem. Phys.* **1999**, *200*, 1333.
[15] A. Finne, A.-C. Albertsson, *Biomacromolecules* **2002**, *3*, 684.
[16] J. Ren, Z. Zhang, Y. Feng, J. Li, W. Yuan, *J. Appl. Polym. Sci.* **2010**, *118*, 2650.
[17] M. Adeli, R. Haag, *J. Polym. Sci., Part A: Polym. Chem.* **2006**, *44*, 5740.
[18] W. Zhang, S. Zheng, Q. Guo, *J. Appl. Polym. Sci.* **2007**, *106*, 417.
[19] E. Vidović, D. Klee, H. Höcker, *J. Polym. Sci., Part A: Polym. Chem.* **2007**, *45*, 4536.
[20] A. Breitenbach, K. F. Pistel, T. Kissel, *Polymer* **2000**, *41*, 4781.
[21] Y.-L. Zhao, Q. Cai, J. Jiang, X.-T. Shuai, J.-Z. Bei, C.-F. Chen, F. Xi, *Polymer* **2002**, *43*, 5819.
[22] C. Gottschalk, F. Wolf, H. Frey, *Macromol. Chem. Phys.* **2007**, *208*, 1657.
[23] Y. Ikada, K. Jamshidi, H. Tsuji, S. H. Hyon, *Macromolecules* **1987**, *20*, 904.
[24] D. Brizzolara, H.-J. Cantow, K. Diederichs, E. Keller, A. J. Domb, *Macromolecules* **1996**, *29*, 191.
[25] M. Kakuta, M. Hirata, Y. Kimura, *Polym. Rev.* **2009**, *49*, 107.
[26] S. C. Schmidt, M. A. Hillmyer, *J. Polym. Sci., Part B: Polym. Phys.* **2001**, *39*, 300.
[27] H. Tsuji, H. Takai, S. K. Saha, *Polymer* **2006**, *47*, 3826.
[28] A. Södergard, M. Stolt, *Prog. Polym. Sci.* **2002**, *27*, 1123.
[29] K. S. Anderson, M. A. Hillmyer, *Polymer* **2006**, *47*, 2030.
[30] P. Song, G. Chen, Z. Wei, Y. Chang, W. Zhang, J. Liang, *Polymer* **2012**, *53*, 4300.
[31] J. Shao, J. Sun, X. Bian, Y. Cui, G. Li, X. Chen, *J. Phys. Chem. B* **2012**, *116*, 9983.
[32] L. Chang, E. M. Woo, *Polym. Eng. Sci.* **2012**, *52*, 1413.
[33] P. Pan, J. Yang, G. Shan, Y. Bao, Z. Weng, Y. Inoue, *Macromol. Mater. Eng.* **2012**, *297*, 670.
[34] S. R. Rathi, E. B. Coughlin, S. L. Hsu, C. S. Golub, G. H. Ling, M. J. Tzivanis, *Polymer* **2012**, *53*, 3008.
[35] N. Othman, C. Xu, P. Mehrkhodavandi, S. G. Hatzikiriakos, *Polymer* **2012**, *53*, 2443.
[36] K. Masutani, C. W. Lee, Y. Kimura, *Macromol. Chem. Phys.* **2012**, *213*, 695.
[37] H. Tsuji, L. Bouapao, *Polym. Int.* **2012**, *61*, 442.
[38] H. Tsuji, Y. Ikada, *Polymer* **1999**, *40*, 6699.
[39] H. Tsuji, Y. Ikada, *Macromolecules* **1993**, *26*, 6918.
[40] H. Tsuji, S. H. Hyon, Y. Ikada, *Macromolecules* **1991**, *24*, 5651.
[41] P. Opaprakasit, M. Opaprakasit, *Macromol. Symp.* **2008**, *264*, 113.
[42] S. Brochu, R. E. Prud'homme, I. Barakat, R. Jerome, *Macromolecules* **1995**, *28*, 5230.
[43] C. L. Wanamaker, W. B. Tolman, M. A. Hillmyer, *Macromol. Symp.* **2009**, *283–284*, 130.
[44] S. Li, M. Vert, *Macromolecules* **2003**, *36*, 8008.
[45] A. O. Fitton, J. Hill, D. E. Jane, R. Millar, *Synthesis* **1987**, *1987*, 1140.
[46] F. Wurm, J. Klos, H. J. Räder, H. Frey, *J. Am. Chem. Soc.* **2009**, *131*, 7954.
[47] D. Wilms, M. Schömer, F. Wurm, M. I. Hermanns, C. J. Kirkpatrick, H. Frey, *Macromol. Rapid Commun.* **2010**, *31*, 1811.
[48] C. Mangold, F. Wurm, B. Obermeier, H. Frey, *Macromol. Rapid Commun.* **2010**, *31*, 258.
[49] M. Schömer, H. Frey, *Macromol. Chem. Phys.* **2011**, *212*, 2478.
[50] S. Rathi, J. P. Kalish, E. B. Coughlin, S. L. Hsu, *Macromolecules* **2011**, *44*, 3410.
[51] G. Maglio, A. Migliozzi, R. Palumbo, *Polymer* **2003**, *44*, 369.
[52] D. Shin, K. Shin, K. A. Aamer, G. N. Tew, T. P. Russell, J. H. Lee, J. Y. Jho, *Macromolecules* **2004**, *38*, 104.
[53] G. Kister, G. Cassanas, M. Vert, *Polymer* **1998**, *39*, 267.
[54] H. Tsuji, *Macromol. Biosci.* **2005**, *5*, 569.